A High-Resolution Temperature-Salinity Dataset Observed by Autonomous Underwater Vehicles for the Evolution of Mesoscale Eddies and Associated Submesoscale Processes in South China Sea

Chunhua Qiu[1,2], Zhenyang Du[1,2], Haibo Tang[1,2], Zhenhui Yi[1,2], Jiawei Qiao[1,2], Dongxiao Wang[1,2,*], Xiaoming Zhai[3], Wenbo Wang[1,2]

1. School of Marine Sciences, State Key Laboratory of Environmental Adaptability for Industrial Products, Sun Yat-Sen University, and Southern Marine Science and Engineering Guangdong Laboratory (Zhuhai), Zhuhai, China

2. Guangdong Provincial Key Laboratory of Marine Resources and Coastal Engineering, School of Marine Sciences, Sun Yat-sen University, Guangzhou 510275, China

3. Centre for Ocean and Atmospheric Sciences, School of Environmental Sciences, University of East Anglia, Norwich, UK

Corresponding author:

Dongxiao Wang

School of Marine Sciences,

Sun Yat-sen University

Email: dxwang@mail.sysu.edu.cn

Abstract. Marginal seas are usually filled with strongly varying mesoscale eddies (MEs), which evolutions plays vital roles in regulating global oceanic energy equilibrium, triggering submesoscale processes with strong vertical velocity, and inducing high biogeochemistry transport. But the temporal evolutions of MEs and submesoscale processes with several kilometers' resolutions are difficult to be measured by traditional observations with passive working mode. The autonomous underwater vehicles (AUVs) and gliders (UGs) actively observe oceanic motion, and could provide us spatiotemporal synchronization information for strongly varying MEs. Here, we present a 9-year high-resolution dataset of AUVs/UGs observations in 2014-2022 in the South China Sea (SCS) that can be downloaded from https://doi.org/10.57760/sciencedb.11996 (Qiu et al., 2024b). In total, 11 cruise experiments were conducted, deploying 50 UGs and 2 AUVs with spatial and temporal resolutions of <7 km and <6 hours. It covers the area of eddy's birth, propagation, and dissipation, presenting us the most complete data to investigate the evolution of MEs at different life stages. 40% of data reach resolutions < 1 km and < 1 hour, which provides us the dynamic characteristics of submesoscale instabilities across and along front at the eddy edge. This dataset has potential in improving the forecast accuracy in physical and biogeochemistry numerical model. Much more aggressive field investigation programs will be promoted by the NSFC in future.

Keywords: Autonomous Underwater Vehicles; Mesoscale eddies; submesoscale processes; South China Sea

1. Background

Evolution of mesoscale eddies (MEs), with strong geostrophic straining rate, favors the generation of submesoscale processes with several kilometers' spatial resolution (McWilliam, 2016), and requires high-accuracy, spatiotemporal synchronization and high-resolution observations. They easily generate by obtaining kinetic energy from large-scale current, and easily dissipate to submeso- or smaller- scale processes at the slope region via shear and baroclinic instabilities (Oey, 1995; Okkonen et al., 2003). Marginal seas (such as, Gulf of Mexico, Mediterranean) are usually filled with MEs (Rossby number $R_o = U/fL \approx 0.1$), and smaller scale processes ($R_o > 1$). MEs are also numerous in the tropical marginal sea of South China Sea (SCS; Chen et al., 2011; Wang et al., 2003; Xiu et al., 2010). They have the spatial scale of 50–300 km and temporal scale of several weeks to months, playing vital roles in the transport of matter and energy (Chelton et al., 2007; Morrow et al., 2004).

Observation platforms for MEs include ship-cruise, satellite, Argo float, mooring, drifters, autonomous underwater vehicles (AUVs), and underwater gliders (UGs), etc. These platforms have been utilized to detect variations of MEs in SCS (Table 1). Ship-cruise observations are the most traditional methods to investigate the MEs' general structures (Wang et al., 1987; Xu et al., 1997), but difficult to track their spatiotemporal evolutions. Satellite data provide wide surface information of MEs (i.e., temporal and spatial scales, eddy radius, tracks; Chelton et al., 2011). Southwest of Taiwan Islands, northwest of Luzon Islands, Xisha Islands region, and east of Vietnam are the four main eddy birth pools (Hwang et al., 2000; Wang et al., 2003; Nan et al., 2011). After birth, MEs move westward, southwestward, or northwestward under the control of the first-baroclinic Rossby wave (Lin et al., 2007; Xiu et al., 2010; Chen et al., 2011). Since 2002, a large number of Argos have been deployed, providing routine measurements to describe vertical structures of MEs (He et al., 2018; Table 1). The spatiotemporal resolutions of Argo profiles are approximately 100 km and 10 days, which is difficult to capture the high-frequency variability of MEs and submesoscale processes (Table 1).

Table 1. Observation studies of MEs in SCS.
MEs: mesoscale eddies; SCS: South China Sea

Platforms	Authors	ME Sources
Ship Observation (CTD Station)	Dale, 1956	Cool pool near Vietnam
	Wang et al., 1987	Warm eddy near southwestern of Taiwan Islands
	Xu et al., 1997	Northwest of Luzon Islands, named Luzon cold eddy
	Li et al., 1998	A warm eddy in northeast of NSCS
	Chu et al., 1998	An eddy pair in central of SCS.
	Fang et al., 2002	Vietnam warm eddy
Satellite Observations (sea level anomaly; velocity)	Hwang et al., 2000; Wang et al., 2003; Nan et al., 2011	Topex/Poseidon altimeter data, 94 cold eddy, 124 warm eddy. Southwest of Taiwan Islands, northwest of Luzon Islands, East of Vietnam.
	Lin et al., 2007; Chen et al., 2011; Xiu et al., 2010	Radius, life cycle, tracking, seasonal and interannual variations of mesoscale eddies
	He et al., 2016	The role of ENSO on interannual variation in Luzon Strait mesoscale eddies
	He et al., 2019	MEs' influence on Chlorophyll-a
Argo; Mooring	Li et al., 2022	Vertical tilt of Mesoscale eddy
	He et al., 2018	Reconstruction data combine altimeter and Argos, revisit the three-dimensional structures of ME
	Zhang et al., 2017	By using mooring array, investigate eddy looping from Luzon Strait

Attributed to the active tracking, AUVs and UGs become more and more important tools in exploring marine environment over last two decades. They have the advantages in low cost, long-duration, controllability and reusability. Our group has collected high-resolution UGs and AUVs observations across MEs. UGs adjust buoyancy to generate gliding motion through water columns by a pair of wings, and have been developed since 2004 (Bachmayer et al., 2004; Caffaz et al., 2010). UGs moves in a sawtooth trajectory at a slow speed of 0.3 m/s, while AUVs are propeller-driven, acting as sawtooth and drifting mode at the maximum speed of 1 m/s (Hobson et al., 2012). It takes around 8/3 days for an UG/AUV to pass a quasi-steady eddy with mean radius of ME (100 km) in SCS. Conductivity-temperature-depth(CTD) are installed on the UGs and AUVs to measure marine temperature and salinity environment. Hence, UGs and AUVs have been successfully used in detecting strongly varying features in some marginal seas, such as the warming trend in Gulf Stream (Todd and Ren, 2023), or the water mass exchanges between Bay of Bengal and Arabian Sea (Rainville et al., 2022). We conducted UGs experiments since 2014 (Qiu et al., 2015), and made AUV experiments since 2018 (Huang et al., 2019; Qiu et al., 2020). Here, we present 9-year (2014-2022) AUVs and UGs datasets in SCS, and try to show their potential abilities in detecting the evolutions of MEs and the associated submesoscale processes.

2. Data Description

2.1 UG and AUV experiment sites

Different with Rainville et al (2022) and Todd and Ren (2023), most of our experiments aimed to detect the evolution of MEs or submesoscale processes. Two products of Chinese UGs named “Sea Wing” (Yu et al., 2011) and “Petrel” (Wu et al., 2011) are utilized in revealing the development of MEs in this study. Since 2014, we have conducted 11 experiments, totally collecting 13491 temperature and salinity profiles, which is even more than those in Gulf Stream (Todd and Ren, 2023). 50 UGs and 2 AUVs were deployed in northern SCS. The deploying time, installed sensors, and diving depths of UGs/AUVs experiment were shown in Table 2. More detailed information, including vehicle serial number, waypoints, matching time, latitude, and longitude is stored in the data with *.NC format. The gray highlighted the UG network experiments, with number of UGs ≥3. Such as, in the experiments of 2017, 2019 and 2020, more than 10 UGs were deployed to detect the three-dimensional structures of the MEs.

Table 2. Information of individual UG/AUV experiment and the observing purpose. ME: Mesoscale Eddies; AUV: Autonomous Underwater Vehicle; UG: Underwater Glider.

Number	Equipment	Time	Number of Qualified Profiles	Number of Eliminated Profiles (Stage)	Number of equipment	Sensor of equipment (*: with Shipped CTD)	Diving depth of equipment	Observing Purpose
1	UG	Sept. 19- Oct. 15, 2014; 26 days	227	0	1 UG	Seabird Glider Payload CTD(GPCTD)	1000 m	Mixed layer heat budget; sea trials
2	UG	Apr. 18-Jul. 6, 2015; 78 days	1358	1(Syntax_Test)	3 UGs Network	Seabird Glider Payload CTD(GPCTD)	1000 m	Structures of ME
3	UG	Jul. 14-UG. 13, 2017 30 days	2902	99(Syntax Test)	10 UGs, Network	Seabird Glider Payload CTD(GPCTD)	300 m (3) 1000 m (7)	ME response to TC
4	UG	Apr. 22-May 23, 2018; 31 days	239	0	1 UG, Virtual mooring	Seabird Glider Payload CTD(GPCTD)	1000 m	Structures of ME
5	UG	Jul. 13- Sept. 30, 2019; 77 days	3672	0	17 UGs, Network	Seabird Glider Payload CTD(GPCTD) *	1000 m (17)	Slope intrusion of ME
6	AUV	Sept. 18- Oct. 23, 2019; 35 days	131	0	1 AUV	SBE37 CTD; DVL^{++}	300 m	Evolution of ME
7	UG	Jun. 26- Aug. 27, 2020; 60 days	3793	7(Syntax Test)	12 UGs	Seabird Glider Payload CTD(GPCTD)	1000 m	Slope current
8	UG	Jul. 26- Aug. 8, 2021; 13 days	307	155(Climatology_Test & Syntax_Test);	2 UGs	RBR legato CTD	300 m (1) 1000 m (1)	Edge of ME
9	UG	Aug. 7- Aug. 27, 2021; 20 days	215	0	2 UGs	Seabird Glider Payload CTD(GPCTD)	1000 m	Edge of ME
10	AUV	May 9- Jul. 29, 2021; 80 days	168	0	1 AUV	SBE37 CTD	300 m	Evolution of ME
11	UG	Jun. 23- Jul. 6, 2022; 13 days	217	0	2 UGs	Seabird Glider Payload CTD(GPCTD)	1000 m	Edge of ME
Total	/	463 days	13229	262	50 UGs, 2 AUVs	/	/	Structures and evolution of ME

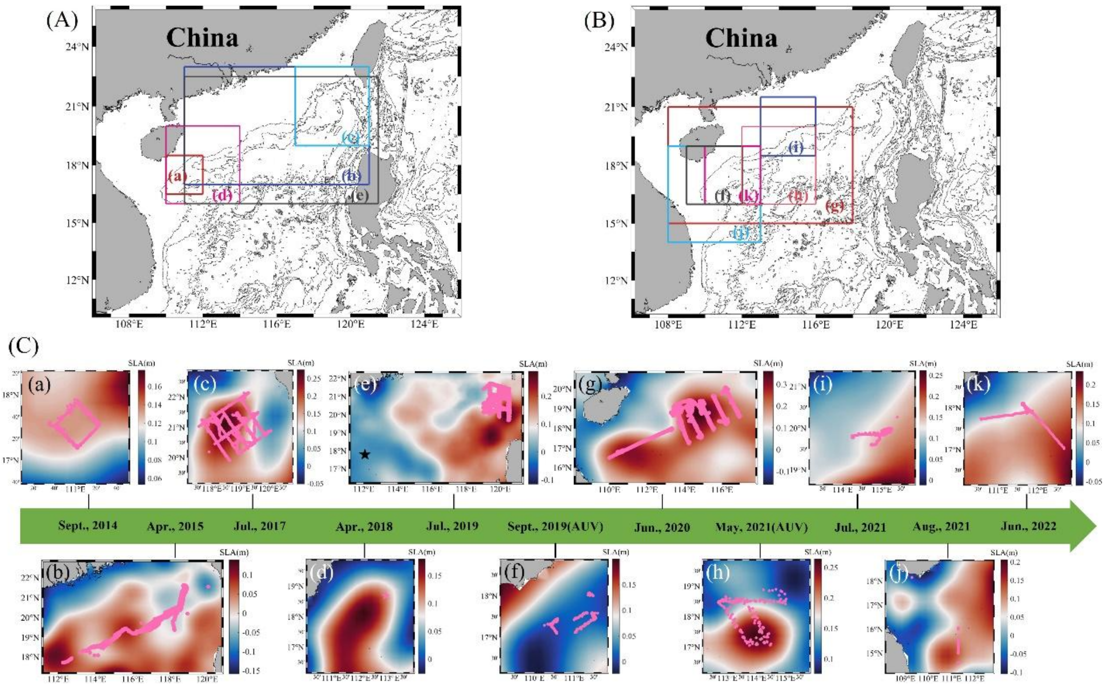

Figure 1. Underwater glider (UG) and autonomous underwater vehicle (AUV) observation sites. (A) observation area for subplots (a)-(e); (B) area for subplots (f)-(j). The grey lines in (A) and (B) are the water depth. (a)-(j) Observation stations (pink dots) with sea level anomaly (SLA averaged over the entire duration of the campaign, shading colors). The observation times are (a) September, 2014; (b) April, 2015; (c) July, 2017; (d) April, 2018; (e) July, 2019; (f) September, 2019; (g) June, 2020; (h) May, 2021; (i) July, 2021; (j) August, 2021; and (k) June, 2022.

2.2 Intercomparison of UGs / AUVs resolution

The UGs and AUVs positions during experiment time were shown in Figure 1. The positive/negative sea level anomaly (SLA) center is the ME center. Note that all the UGs and AUVs crossed MEs. The spatial and temporal resolutions of samples were presented in Figure 2. The dominant spatial resolution (blue bars) was 4-7 km in 2014, 2015, and 2019, while it was smaller than 3 km in other years. In 2017 (Figure 2c), July 2021 (Figure 2f) and 2022 (Figure 2h), the temporal resolution of UGs achieved 1-2 hours, while it was 4-7 hours in other experiments. It indicates that all of the experiments could resolve the MEs (spatial scale of 50-300 km), and 40% of them could be used to resolve submesoscale processes (spatial scale of <3 km).

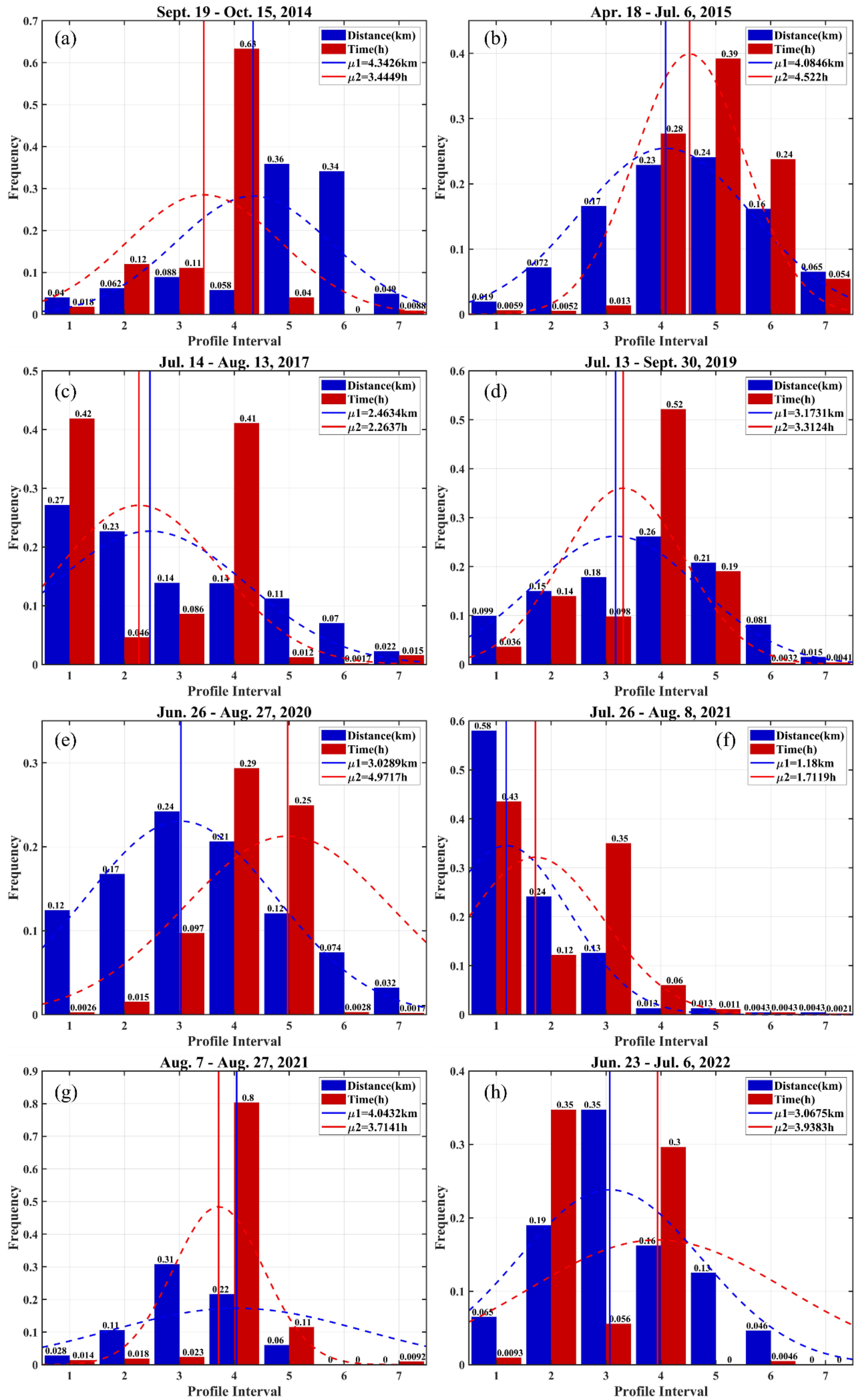

Figure 2. Frequency of spatial (blue bar) and temporal (red bar) sample interval. The red and blue bars (dashed red and blue lines) denote probabilities of spatial and time interval (the normal distributions of spatial and time intervals), respectively.

3 Data Quality Control Method

Before investigating the three-dimensional structures of MEs, we did data quality-control for the UGs and AUVs.

3.1 Quality control for UG data

Two products of Chinese UGs named “Sea-wing” and “Petrel” were used in this study. The communication and navigation subsystem contain iridium satellite communication devices, wireless communication devices, a precision navigation attitude sensor, a Global Positioning System (GPS) device, a pressure meter, and an obstacle avoidance sonar. A CTD sensor with ~6 s sampling resolutions has been installed on the two UG products.

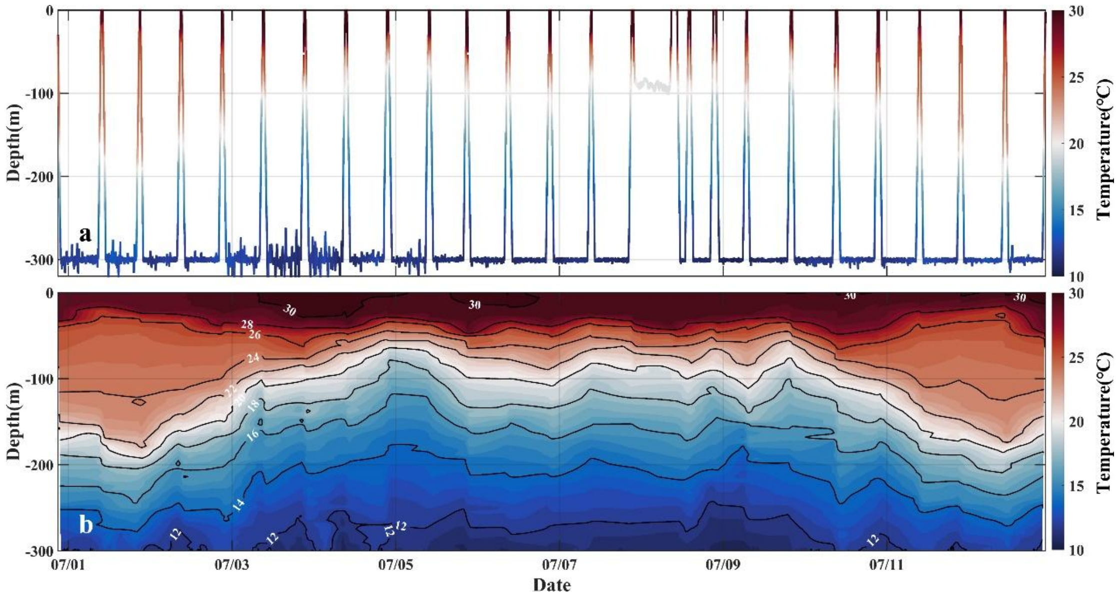

Figure 3. Illustration of (a) original, and (b) interpolated data after quality control. The AUV duration is in July 2021. AUV: autonomous underwater vehicle.

Before investigating oceanic phenomena, we did data quality control following the standard of integrated ocean observing system (IOOS). The quality-control procedure for UG (https://repository.oceanbestpractices.org/handle/11329/289?show=full) includes 9 steps: (1) Timing/Gap Test: Test determines that the profile has been received within the expected time window and has the correct time stamp; (2) Syntax Test: Ensures the structural integrity of data messages; (3) Location Test: Test if the reported physical location (latitude and longitude) is within the reasonable range determined by the operator; (4) Gross Range Test: Ensure that the data points do not exceed the minimum/maximum output range of the sensor; (5) Pressure Test: Test if the pressure records increase monotonically with depth, sorted the vertical depth values and removed any duplicate depth values; Data after steps (1)-(5) are directly output from UGs. (6) Climatology Test: Test if the data points are within the seasonal expectation range; (7) Spike Test: Test if the data points exceed the selected threshold compared to adjacent data points, excluded the data with temperature/salinity larger than 35 ℃ /35 psu. In steps (6) & (7), we exclude abnormal values of temperature/salinity, and produce data named "*_RO" ; (8) Rate of Change Test: Test if the rate of change in the time series exceeds the threshold determined by the operator; (9) Flat Line Test: Test for continuously repeated observations of the same value, which may be the result of sensor or data collection platform failure. Then the data beyond three standards deviations of steps (8)-(9) are excluded. These data were produced and named "*_TSD".

We have validated the UG observed temperature and salinity profiles with ship observed data during July, 2019 (black star in Figure 1e; Figure 4). The mean bias of temperature is 0.05 ℃, and that of salinity is 0.01 psu. The vertical temperature/salinity profiles observed by ship and UG installed CTD are consistent, supporting that the data are credible.

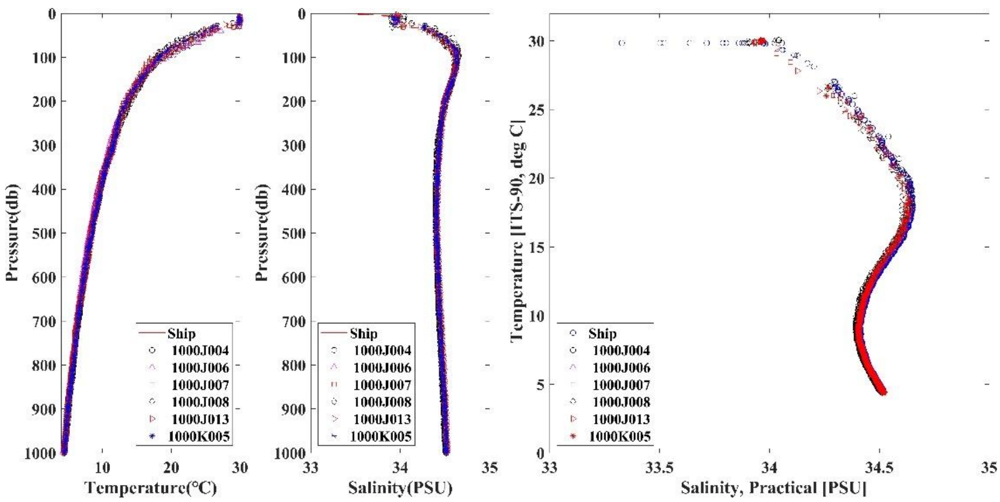

Figure 4. Comparison of (a) temperature, (b)salinity, and (c) temperature-salinity scatter plots between ship installed CTD and AUV installed CTD at station (112.0661°E, 17.7778°N). Red line in (a) and (b) is the ship measured values. Dot, green triangle, red square, diamond, red triangle, and blue star are for UGs named 1000J004, 1000J006, 1000J007, 1000J008, 1000J013 and

1000K005, respectively.

3.2 Quality control for AUV data

Both CTD and GPS instrument were installed on the "Sea-Whale 2000" AUV. This AUV was designed by Institute of Shenyang Automation, Chinese Academy of Sciences. It could operate in two modes, a "sawtooth-like" mode and a "cruise" mode at a depth of 300 m (Huang et al., 2019).

In the "sawtooth-like" mode, the data quality control procedures are the same as those for UGs. Figures 3 and 4 show the AUV observed temperature after data quality-control. In "cruise" mode, the AUV navigates at the depth of around 300 m. Following Qiu et al (2020), we firstly transformed the temperature and salinity at depth z to those at 300 m using a linear regression method ($T' = 0.008\mathrm{z}' + 0.017; S' = -0.0002z' + 0.0006$),

$$T' = T_z - T_{mean}, \tag{1a}$$

$$S' = S_z - S_{mean}, \tag{1b}$$

where T_{mean} is averaged using a 10-point smooth average, which could maintain the spatial variations from 20 to 30 km. Depth anomaly is defined as the measured depth minus 300 m, $z' = z - 300$, and the temperature and salinity anomalies as $T'$and S', respectively. We compared this method with the potential temperature algorithm, and the temperatures obtained at 300 m were highly consistent.

3.3 Density derived from temperature and salinity

The value of seawater density (ρ, in kg/m^3) can be calculated based on temperature (T in °C), salinity (S in psu), and pressure (P in dbar). The UNESCO formula provides a simplified approach to estimate seawater density as follows:

$$\rho(S,T,P) = \frac{\rho_0(S,T)}{1 - \frac{P}{K(S,T,P)}} \tag{2a}$$

$$\rho_0(S,T) = \rho_{sw}(T) + (b_0 + b_1T_{68} + b_2T_{68}^2 + b_3T_{68}^3 + b_4T_{68}^4)S + (c_0 + c_1T_{68} + c_2T_{68}^2)S\sqrt{S} + d_0S^2 \tag{2b}$$

$$\rho_{sw}(T) = a_0 + a_1T_{68} + a_2T_{68}^2 + a_3T_{68}^3 + a_4T_{68}^4 + a_5T_{68}^5 \tag{2c}$$

$$T_{68} = T \times 1.00024 \tag{2d}$$

where $K(S, T, P)$ is secant bulk modulus, a_0 and others are coefficients. This formula accounts for the haline and thermal contraction of seawater. The detailed method is as per Fofonoff and Millard (1983).

4. Data Application

4.1 Intra-thermocline (Subsurface) MEs observed by UGs and AUVs

Cross-eddy tracks of UG or AUV could observe both the warm core and cold cores (Figure 4). In April 2015, one UG crossed a warm eddy, and observed a subsurface warm core (Figures 1b & 5a). The warm core ranges from 50-500 m depth with horizontal radius about 100 km, which is termed as intra-thermocline anticyclone and has been reported in Shu et al (2016). Qiu et al (2019) utilized the same experimental dataset to investigate the asymmetry structures of this intra-thermocline eddy, suggesting that the centrifugal force should be taken into account when revealing the velocity of MEs, i.e. gradient wind theory. This gradient wind theory has been cited in a deriving global cyclogeostrophic currents data (Cao et al. 2023). In June 2020 (Figures 1g & 5d-f), one UG captured an intra-thermocline cold eddy with a negative temperature and positive salinity anomaly core, inducing a high-density core. The anomaly is defined as the value minus the zonal mean value. And the high-density core ranged from surface to 500 m depth. Above all, single UG/AUV could capture both the surface and the intra-thermocline eddy's position, range and strength.

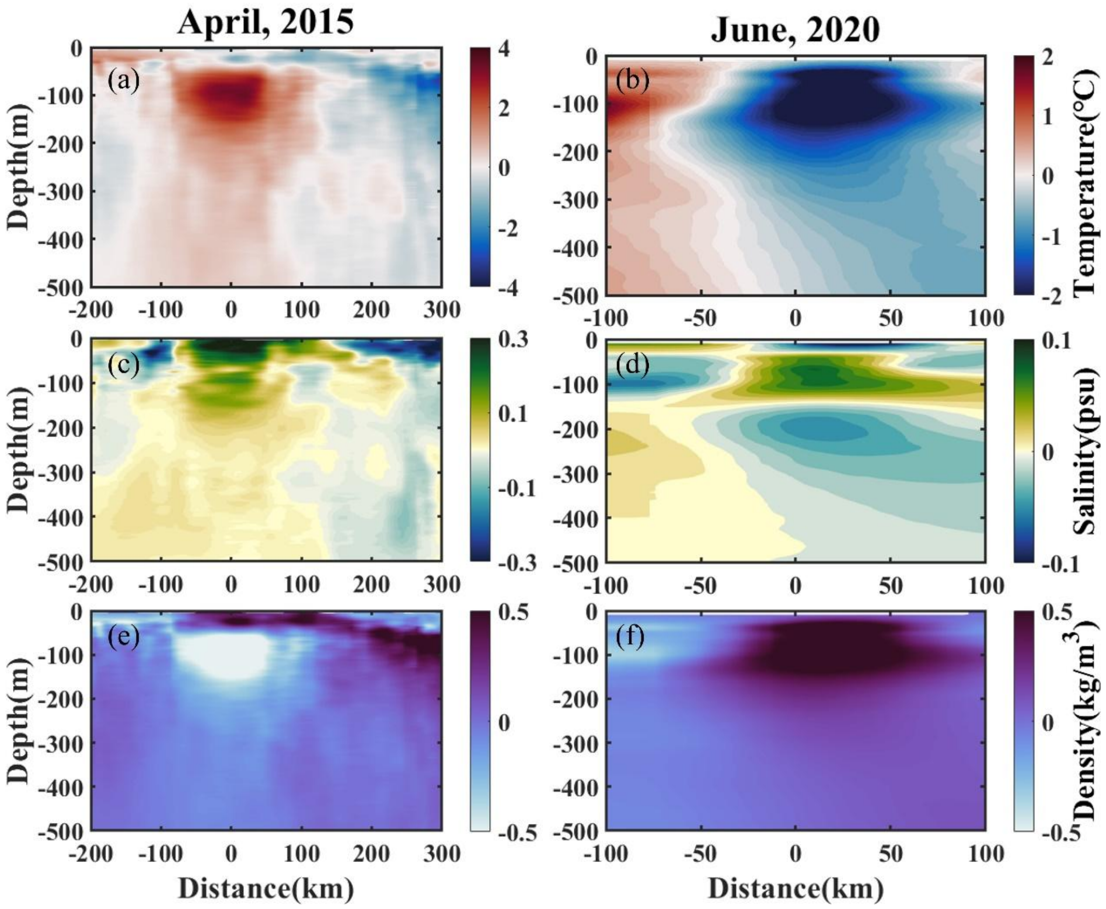

Figure 5. Contour of (a) and (b) temperature anomaly (c) and (d) salinity anomaly, (e) and (f) density anomaly in April, 2015(left panels) and June, 2020(right panels). The contours were generated using interpolation of the original data points.

UG/AUV could track the development of intra-thermocline MEs. During developing stage, MEs can easily deform ,causing cross-slope transports at the continental slope (Wang et al., 2018; Su et al., 2020; Qiu et al., 2022), and produce submesoscale process (Dong et al., 2018; Yang et al., 2019). To observe the development of ME, an AUV has traversed an anticyclonic ME using 5 repeated rectangular tracks from May to July 2021(Figure 1h). This experiment was supported by National Key R&D Program.

In Figure 6, we show an anticyclonic eddy located in the subsurface layer at a depth of 50-200 m, characterized by a low Brunt-Väisälä frequency squared value ($N^2 = \frac{1}{\rho}\frac{d\rho}{dz} < 10^{-4}$), existing as an intra-thermocline anticyclonic eddy. The repeated cruise of AUV was separated to five stages, termed as T1(June 8-11), T2 (June 19-23), T3

(June 29- July 4), T4 (July 10- 15), and T5 (July 21-26). Taking 22.5 kg/m^3 and 23.5 kg/m^3 as the upper and lower boundary of the intra-thermocline ME, we calculated the area and the mean temperature within the ME. The area and mean temperature decreased from T1-T3, and then increased from T4-T5, indicating this anticyclonic eddy weakened from T1-T3 and strengthened from T4-T5. The development of this eddy has been described in detail by Qiao et al (2023), who found it moved eastward during T1-T3 and got stuck during T4-T5.

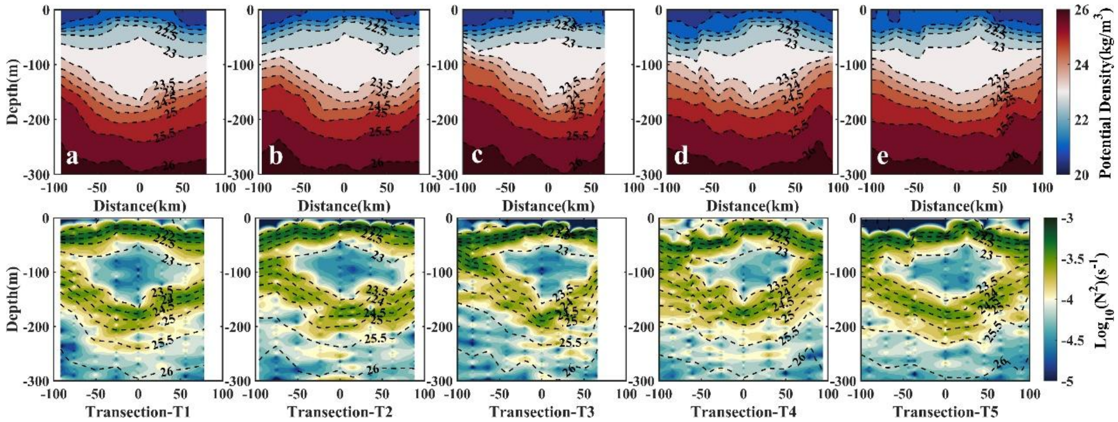

Figure 6. The profiles of density (upper panel) and Brunt frequency (lower panel) during (a,f)T1, (b,g)T2, (c,h)T3, (d, i)T4, (e, j)T5 period, which was 06/08-06/11,06/19-06/23,06/29-07/04,07/10-07/15,07/21-07/26, respectively. The contours were generated using interpolation of the original data points.

4.2 Vertical Tilt of MEs at different life-stages observed by UGs

Several systematic UG campaigns were conducted in 2015, 2017, 2019, and 2020. A whole life cycle of ME usually experiences birth, developing, mature and dissipate stages (Zhang and Qiu, 2018; Yang et al., 2019), and the eddy's life stage has suggested to influence on the kinetic energy change of MEs. Luzon strait is an eddy birth zone, where Kuroshio branch intrudes the SCS (Chen et al., 2011; Su et al., 2020). After birth, most of the eddies move westward to the continental shelf zone under the modulation of Rossby wave, finally dissipate in Dongsha Islands, Xisha Islands or merged with other eddies (Yang et al., 2019; Su et al., 2020; Qiu et al., 2022).

The systematic UG experiments provide us probability in capturing the different vertical structures of MEs at different life stages. After data quality-control, we firstly mapped the temperature and salinity data onto 1 km × 1 km × 1 m grid, and then calculated the water density, ρ. The ME follows geostrophic balance, thus the geostrophic velocity could be derived under the force balances between pressure gradient and Coriolis force. We derived the geostrophic velocity, v_g, by using thermal-wind relationships,

$$v_g(x,y,z) = v_0 - \frac{g}{f\rho_0}\int_{z0}^{z}\left(\frac{\partial\rho(x,y,z)}{\partial x} + \frac{\partial\rho(x,y,z)}{\partial y}\right)dz, \quad (3)$$

where ρ_0 is the referenced water density, f is the Coriolis frequency, v_0 is the referenced geostrophic velocity at depth 1000 m and assumed to be 0.

Figure 7a-b depicts the three-dimensional temperature and geostrophic velocity structures of a ME (120 °E) at birth stage, as observed by 12 UGs in July 2019 (Figure 1e&6a-b). A warm core was located at subsurface layer and the eddy center exhibited a northeastward vertical tilt (solid black line). In July 2017 (Figures 1c & 6c-d), 10 UGs were deployed westward to the Luzon Strait (119 °E). This eddy was in its developing phase and possessed a significant eastward vertical tilt from deep up to surface, reaching depths deeper than 500 m. The eastward vertical tilt is suggested to have been induced by the background current, westward propagation of Rossby Waves (e.g., Qiu et al., 2015; Zhang et al., 2016; Li et al., 2019), and advection background temperature gradient (e.g., Bonnici and Billant, 2020; Gaube et al., 2015; Li et al., 2020). Throughout this experiment, the UGs encountered the tropical storm "Haitang", results in that the ME underwent horizontal deformation, giving rise to submesoscale processes (Yi et al., 2022; Yi et al., 2024).

In June 2020, 12 UGs were deployed across an anticyclonic ME in the shelf region (Figures 1g and 6e-h). The eddy was under dissipating stage due to the steep topography, displaying a significant southwestward tilt from a depth of 500 m to surface (Figure 7e-7f). This kind of southwestward vertical tilt was revealed by potential vorticity in a numerical model (Qiu et al., 2022), which was attributed to shallower water depth to the west of MEs, and caused asymmetries of the velocities within the MEs. Qiao et al (2023) also captured an eastward movement of a ME by using AUV observations in June 2021(Figure 1h). Based on tensor decomposition of barotropic instability energy, they suggested wave-current interaction played the most important role in the development and propagation of this eddy.

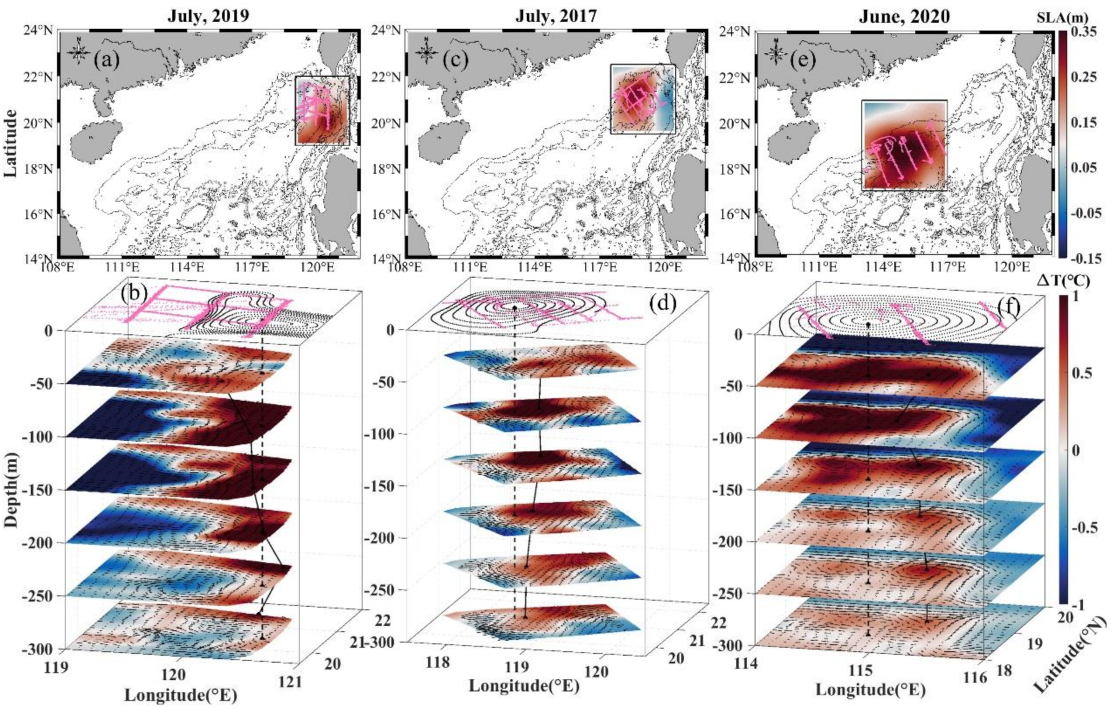

Figure 7. Eddy structures during periods of (a-b) eddy birth, (c-d) westward movement, and (e-f) dissipation along slope movements. Sea level anomaly (SLA) and UGs' positions are superimposed in upper panels (a, c, e), isobaths are represented by solid lines. The UG observed temperature and derived geostrophic velocities are in the 3D plots (b, d, f). Pink lines are the tracks of UGs. Dashed lines denote the centers of mesoscale eddies from SLA fields, and solid dot lines are the centers from warm cores. UG: Underwater Glider. The contours were generated using interpolation of the original data points.

4.3 Submesoscale instabilities at the edge of MEs observed by UGs

Smaller-scale structures, i.e., submesoscale process, usually occurs within MEs, either at the eddy edge (front; filament) or entrained in the eddy center, in terms of spiral structures or "eye-cat" structures (Zhang and Qiu, 2018; Ni et al., 2021; Hu et al., 2023; Qiu et al., 2024). They could cascade kinetic energy downward to turbulent scale via symmetric or centrifugal instabilities, and also induce kinetic energy inverse cascade to MEs via mixed layer baroclinic instabilities (i.e., Fox-Kemper et al., 2008; McWilliams, 2016). However, the submesoscale processes within MEs are difficult to be observed by Argo with 10-day's temporal resolution. Tang et al (2022) observed submesoscale fronts using NAVIS float, and found that mixed-layer baroclinic instability dominated this frontogenesis. Qiu et al (2019) and Shang et al (2023) have captured a submesoscale front at the eddy's edge by using a "virtual mooring" UG observation. As passively driven by flow, NAVIS can only observe submesoscale process in an approximate Lagrangian fashion, whereas UGs could provide us both the cross-front and along-front information, depending on our observational scheme.

In our datasets, 40% of UG observations have high spatiotemporal resolutions (<3 km, <4 h; Figure 2), which are fine enough to capture the submesoscale processes. Here, we present two examples of submesoscale instabilities at the edge of MEs to show the advantages of UG observations.

As shown in Figure 8a, 4 UGs were deployed at the eddy's edge (front) in 2017. 3 UGs crossed the front and 1 UG tracked along the front. Following Thomas et al (2013), the converted angle of the Richardson number, ϕ_{Ri}, can also be used to determine the nature of the instability:

$$\phi_{Ri} = tan^{-1}\left(-\frac{1}{Ri}\right) = tan^{-1}\left(\frac{|\nabla \cdot b|^2}{N^2 \cdot f^2}\right), \tag{3a}$$

$$Ri \approx Ri_g = \frac{N^2}{\left(\frac{\partial \overline{v_g}}{\partial z}\right)^2} = \frac{N^2 \cdot f^2}{|\nabla \cdot b|^2} < \frac{f}{\zeta_g}, \text{ and } f \cdot \zeta_g > 0. \tag{3b}$$

where $b = -g\rho/\rho_0$, is the buoyancy flux, g is the gravitational acceleration. $N^2 = \partial b/\partial z$ is the vertical buoyancy frequency. $\zeta_g = curl(\overrightarrow{v_g})$ is the vertical relative vorticity. For anticyclonic eddies, inertial instability or symmetric instability occurs when $-45° < \phi_{Ri} < \phi_c$; symmetric instability occurs when $-90° < \phi_{Ri} < -45°$; symmetry instability or gravitational instability occurs when $-135° < \phi_{Ri} < -90°$; and gravitational instability occurs when $-180° < \phi_{Ri} < -135°$.

Figure 8a shows that UGs observed several types of submesoscale instabilities, in terms of gravity instability, symmetric instability and mixed instabilities from symmetric and centrifugal instabilities at the anticyclonic eddy's edge. Figure 8b shows submesoscale instabilities in 2019. In this case, gravity instability dominates the upper mixed layer, while symmetric and centrifugal instabilities are not significant. These two cases provide us enough information to detect frontal genesis processes in Eulerian view, while NAVIS or Argos provide frontal information in Lagrange view.

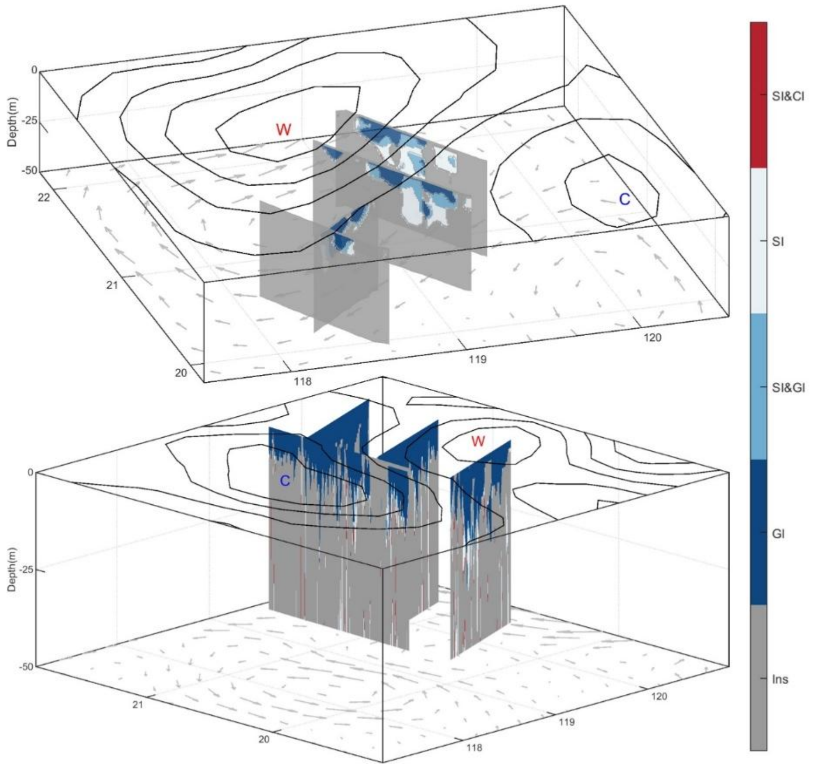

Figure 8. Analyzed submesoscale instabilities at the edge of mesoscale eddies. (a)in 2017, and (b) in 2019. SI: symmetric instability; CI: centrifugal instability; GI: gravity instability. W: anticyclonic eddy; C: cyclonic eddy. Isolines are the sea level anomaly. The contours were generated using interpolation of the original data points.

5. Data availability

The dataset of temperature/salinity observed by AUV and UG in this manuscript was deposited in Science Data Bank, whose DOI is https://doi.org/10.57760/sciencedb.11996 (Qiu et al., 2024b). The dataset includes two files of “Grid_data” and “Observation_data”.

6. Conclusions and Potential Future Plan

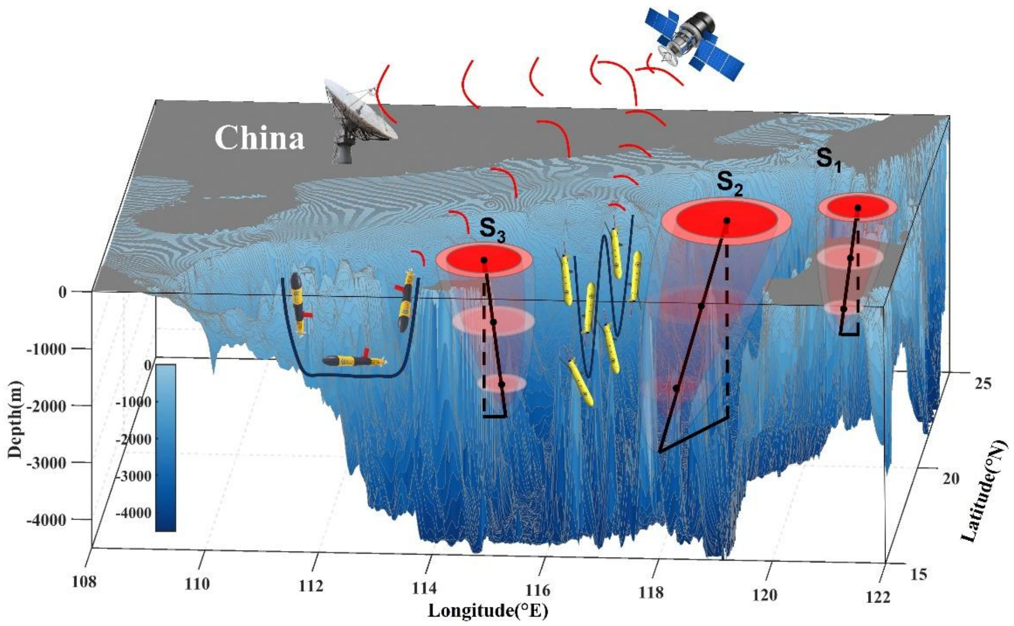

Figure 9. Scheme of UGs observed mesoscale eddies at different life stages in the northern SCS. S1: birth stage; S2: developing/mature stage; S3: dissipating stage. UG: Underwater Glider; SCS: South China Sea.

Based on 9-year AUVs and UGs observations, we obtained high-resolution temperature and salinity profiles datasets in SCS. The dataset provides 13491 profiles and covers 463 days' experiments, including 11 experiments from 50 UGs and 2 AUVs. To our knowledge, the 9-year dataset is enough in detecting the horizontal asymmetry, vertical tilt, temporal evolution, life cycle of MEs (Figure 9), and the associated submesoscale processes. The dataset allows us to investigate the subsurface MEs, revealing eddy-current and eddy-topography interactions successfully. However, to understand the feedback of MEs to the variability of larger scale current, i.e. western boundary current, long-term routine UGs and AUVs observations are needed in future.

Besides tracking MEs, UGs and AUVs have been proved to actively capture smaller scale oceanic process, such as internal tide (Gao et al., 2024), turbulence by using turbulent parameterization schemes (Qi et al, 2020). Moreover, UGs/AUVs equipped with more sensors could also provide us geochemical parameters (e.g., Yi et al., 2022), presenting the potential ability in improving the forecast accuracy in physical and biogeochemical numerical model. More projects gathering AUVs network are ongoing and will be promoted in future.

During the mission, we met some challenges: (1) under strong background current, UGs and AUVs get disturbed and cannot follow the customized routes; (2) bad weather makes it difficult for piloting team to deploy and recovery UGs and AUVs; (3) data receiving capacity depends on the satellite transmission capacity. If both the bio-chemistry and CTD data are included, the data resolution have to be lowered. These challenges require piloting team and oceanographers to work together.

Author contributions

Conceptualization: DX; data curation: CH, ZY, ZH, JW; formal analysis: CH, ZY; funding acquisition: CH, DX; investigation: CH, DX; methodology: CH, DX; project administration: CH, DX; software: CH, DX; supervision: CH, DX; validation: XM, DX, WB; writing: CH, XM. All the authors have read and agreed to the published version of the manuscript.

Financial support

This study was supported by the National Natural Science Foundation of China (Grant No. 42376011), National Key R&D Plan Program (No.2017YFC0305804).

Competing interests

The contact author has declared that none of the authors has any competing interests.

Acknowledgements

We acknowledge all the colleagues and project members who have contributed to the design of UGs and AUVs, the sea experiments and data processing in the past. Many scientists and engineers have participated in active surveys and mappings. Their work provided basic high-quality materials.

Disclaimer

Publisher's note: Copernicus Publications remains neutral with regard to jurisdictional claims made in the text, published maps, institutional affiliations, or any other geographical representation in this paper. While Copernicus Publications makes every effort to include appropriate place names, the final responsibility lies with the authors.

References:

Bachmayer, R., Leonard, N. E., Graver, J., Fiorelli, E., Bhatta, P. and Paley, D. Underwater glider: Recent developments and future applications, *Proceedings of the 2004 International Symposium on Underwater Technology*, 2004, 195~200. https://doi.org/10.1109/UT.2004.1405540.

Caffaz, A., Caiti, A., Casalino, G. and Turetta, A. The hybrid glider/AUV folaga, *IEEE Robotics and Automation Society*, 2010, 17(1), 31~44. https://doi.org/10.1109/MRA.2010.935791.

Cao, Y., Dong, C., Stegner, A., Bethel, B. J., Li, C., Dong, J., et al. (2023). Global sea surface cyclogeostrophic currents derived from satellite altimetry data. *Journal of Geophysical Research: Oceans*, 128, e2022JC019357. https://doi.org/10.1029/2022JC01935

Chen, G., Hou, Y., Chu, X. Mesoscale eddies in the South China Sea: Mean properties, spatiotemporal variability, and impact on thermohaline structure. *Journal of Geophysical Research-Oceans*, 2011, 116, C06018. https://doi.org/10.1029/2010JC006716

Chelton, D., Schlax, M., Samelson, R., de Szoeke, R. Global observations of large oceanic eddies. *Geophysical Research Letters*, 2007, *34*(15), L15606. https://doi.org/10.1029/2007GL030812

Chelton, D., Schlax, M., Samelson, R. Global observations of nonlinear mesoscale eddies. *Progress in Oceanography*, 2011, 91 (2): 167–216, doi:10.1016/j.pocean.2011.01.002.

Chu, P., Chen, Y., Lu, S. Wind-driven South China Sea deep basin warm-core/cool-core eddies. *Journal of Oceanography*, 1998, 54(4), 347-360. doi: 10.1007/bf02742619.

Chu, P., Fan, C. Optimal linear fitting for objective determination of ocean mixed layer depth from glider profiles. *Journal of Atmospheric and Oceanic Technology*, 2010, 27, 1893–1898.

Dale, W. Winds and drift currents in the South China Sea. *Malayan Journal of Tropical Geography*, 1956, 8, 1-31.

Dong, C., Mcwilliams, J., C., Liu, Y., Chen D. Global heat and salt transports by eddy movement. *Nature Communications*, 2014, 5(2), 3294.

Dong, J., Zhong, Y. The spatiotemporal features of submesoscale processes in the northeastern South China Sea. *Acta Oceanology Sinica*, 2018, 37(11), 8-18. https://doi.org/10.1007/s13131-018-1277-2.

Eriksen, C. C., Osse, T. J., Light, R. D., Wen, T., Lehmann, T. W., Sabin, P. L., Ballard, J. W. and Chiodi, A. M. Seaglider: A long range autonomous underwater vehicle for oceanographic research, *IEEE Journal of Oceanic Engineering*, 2001, 26(4), 424~436. https://doi.org/ 10.1109/48.972073.

Fang, W., Fang, G., Shi, P., Huang, Q., Xie, Q. Seasonal structures of upper layer circulation in the southern South China Sea from in situ observations. *Journal of Geophysical Research: Oceans*, 2002, 107(C11), 23-1-23-2. doi: 10.1029/2002JC001343.

Fox-Kemper, B., Ferrari, R., Hallberg, R. Parameterization of mixed layer eddies. Part I: Theory and diagnosis. *Journal of Physical Oceanography*, 2008, 38(6), 1145-1165. https://doi.org/10.1175/2007JPO3792.1

Gao, Z., Chen, Z., Huang, X., Yang, H., Wang, Y., Ma, W., & Luo, C. (2024). Estimating the energy flux of internal tides in the northern South China Sea using underwater gliders. *Journal of Geophysical Research: Oceans*, 129, e2023JC020385. https://doi.org/10.1029/ 2023JC020385

He, Q., Zhan, H., Cai, S., He, Y., Huang, G., Zhan, W. A new assessment of mesoscale eddies in the South China Sea: surface features, three-dimensional structures, and thermohaline transports. *Journal of Geophysical Research: Oceans*, 2018, 123(7), 4906-4929.

https://doi.org/10.1029/2018JC014054

He, Q., Zhan, H., Xu, J., Cai, S., Zhan, W., Zhou, L., Zha, G. Eddy-induced chlorophyll anomalies inthe western South China Sea. *Journal of Geophysical Research: Oceans*, 2019, 124, https://doi.org/10.1029/2019JC015371.

He, Y., Xie, J., Cai, S. Interannual variability of winter eddy patterns in the eastern South China Sea. *Geophysical Research Letters*, 2016, 43(10), 5185-5193. doi: 10.1002/2016GL068842.

Hobson, B. W., Bellingham, J. G., Kieft, B., McEwen, R., Godin, M. and Zhang, Y. Tethys-class long range AUVs - extending the endurance of propeller-driven cruising AUVs from days to weeks. *2012 IEEE/OES Autonomous Underwater Vehicles (AUV)*, 2012, 1-8, https://doi.org/10.1109/AUV.2012.6380735.

Hu, Z., Lin, H., Liu Z., Cao Z., Zhang F., Jiang Z., Zhang Y., Zhou K., and Dai M. Observations of a filamentous intrusion and vigorous submesoscale turbulence within a cyclonic mesoscale eddy, *Journal of Physical Oceanography*, 2023, 53(6), 1615–1627.

Huang, Y., Qiao, J., Yu, J., Wang, Z., Xie, Z., Liu, K. Sea-Whale 2000: a long-range hybrid autonomous underwater vehicle for ocean observations. *OCEANS 2019 - Marseille*, Marseille, France, 2019, 1-6, doi: 10.1109/OCEANSE.2019.8867050.

Hwang, C., Chen, S. Circulations and eddies over the South China Sea derived from TOPEX/Poseidon altimetry. *Journal of Geophysical Research: Oceans*, 2000, 105(C10), 23943-23965. doi: 10.1029/2000JC900092.

Li, H., Xu, F., Wang, G. Global mapping of mesoscale eddy vertical tilt. *Journal of Geophysical Research: Oceans*, 2022, 127, e2022JC019131. https://doi.org/10.1029/2022JC019131

Li, L., Worth. D., Nowlin, J., Su. J. Anticyclonic rings from the Kuroshio in the South China Sea. *Deep Sea Research Part I*, 1998, 45, 1469-1482. doi: 10.1016/s0967-0637(98)00026-0.

Lin, X., Dong, C., Chen, D., Liu, Y., Yang, J., Zou, B., Guan, Y. Three-dimensional properties of mesoscale eddies in the South China Sea based on eddy-resolving model output. *Deep-Sea Research Part I: Oceanographic Research Papers*, 2015, 99, 46-64. https://doi.org/10.1016/j.dsr.2015.01.007

Lin, P., Wang, F., Chen, Y., & Tang, X. Temporal and spatial variation characteristics of eddies in the South China Sea I: Statistical analyses. Acta Oceanologica Sinica,2007, 29(3), 14-22.

McWilliams, J. Submesoscale currents in the ocean. *Proceedings of the Royal Society A,* 2016, 472, 20160117. http://dx.doi.org/10.1098/rspa.2016.0117

Morison, J., Andersen, R., Larson, N., D'Asaro, E., Boyd, T. The correction for thermal-lag effects in Sea-Bird CTD data. *Journal of Atmospheric and Oceanic Technology*, 1994, 11, 1151–1164, https://doi. org/10.1175/1520-0426(1994)011,1151:TCFTLE.2.0.CO;2.

Morrow, R., Birol, F., Griffin, D., Sudre, J. Divergent pathways of cyclonic and anti-cyclonic ocean eddies. *Geophysical Research Letters*, 2004, *31*(24), L24311. https://doi.org/10.1029/2004gl020974

Nan, F., He, Z., Zhou, H., Wang, D. Three long-lived anticyclonic eddies in the northern South China Sea. *Journal of Geophysical Research: Oceans*, 2011, 116(5), C05002. https://doi.org/10.1029/2010JC006790

Ni, Q., Zhai, X., Wilson, C., Chen, C., Chen, D. Submesoscale eddies in the South China Sea. *Geophysical Research Letters*, 2021, 48, e2020GL091555. https://doi.org/10.1029/2020GL091555

Oey, L. Eddy- and wind-forced shelf circulation. *Journal of Geophysical Research*, 1995, *100*(C5), 8621–8637.https://doi.org/10.1029/95JC00785.

Okkonen, S., Weingartener, T., Danielson, S., Musgrave, D., Schmidt, G. M. Satellite and hydrographic observations of eddy-induced shelf-slope exchange in the northwestern Gulf of Alaska. *Journal of Geophysical Research*, 2003, *108*(C2), 3033. https://doi.org/10.1029/2002JC001342.

Osse, T. J. and Eriksen, C. C. The deepglider: a full ocean depth glider for oceanographic research. *OCEANS 2007*, 2007, 1~12. https://doi.org/10.1109/OCEANS.2007.4449125.

Qi, Y., Shang, C., Mao, H., Qiu, C., Shang, X. Spatial structure of turbulent mixing of an anticyclonic mesoscale eddy in the northern South China Sea. *Acta Oceanologica Sinica*, 2020, 39(11), 69-81. https://doi.org/10.1007/s13131-020-1676-z.

Qiao, J., Qiu, C., Wang, D., Huang, Y., Zhang, X., Huang, Y. Multi-stage Development within Anisotropy Insight of an Anticyclone Eddy Northwestern South China Sea in 2021. *Geophysical Research Letter*, 2023, doi:10.1029/2023GL104736

Qiu, C., Mao, H., Yu, J., Xie, Q., Wu, J., Lian, S., Liu, Q. Sea surface cooling in the Northern South China Sea observed using Chinese Sea-wing Underwater Glider Measurements. *Deep Sea Research Part I: Oceanographic Research Papers*, 2015, 105, 111-118.

Qiu, C., Mao, H., Liu, H., Xie, Q., Yu, J., Su, D., Ouyang, J., Lian, S. Deformation of a warm eddy in the northern South China Sea. *Journal of Geophysical Research: Oceans*, 2019, 124, 5551-5564. https://doi.org/10.1029/2019JC015288

Qiu, C., Mao, H., Wang, Y., Su, D., Lian, S. An irregularly shaped warm eddy observed by Chinese underwater gliders. *Journal of Oceanography*, 2019, 75, 139-148.

Qiu, C., Liang, H., Huang, Y., Mao, H., Yu, J., Wang, D., Su, D. Development of double cyclonic mesoscale eddies at around Xisha Islands observed by a 'Sea-Whale 2000' autonomous underwater vehicle. *Applied Ocean Research*, 2020, https://doi.org/10.1016/j.apor.2020.102270.

Qiu, C., Yi, Z., Su, D., Wu, Z., Liu, H., Lin, P., He, Y., Wang, D. Cross-slope heat and salt transport induced by slope intrusion eddy's horizontal asymmetry in the northern South China Sea. *Journal of Geophysical Research: Oceans,* 2022, doi: 10.1029/2022JC018406.

Qiu, C., Yang, Z., Feng, M., Yang, J., Rippeth, T.P., Shang, X., Sun, Z., Jing, C., Wang, D. Observational energy transfers of a spiral cold filament within an anticyclonic eddy. *Progress in Oceanography*, 2024a, https://doi.org/10.1016/j.pocean.2023.103187**.**

Qiu, C., Du, Z., Tang, H., et al. UG and AUV data used in research "A High-Resolution Temperature-Salinity Dataset Observed by Autonomous Underwater Vehicles for the Evolution of Mesoscale Eddies and Associated Submesoscale Processes in South China Sea " [DS/OL]. V2. Science Data Bank, 2024b[2024-08-03]. https://doi.org/10.57760/sciencedb.11996. DOI: 10.57760/sciencedb.11996.

Rainville, L., Lee, C., Arulananthan, K., Jinadasa, S., Fernando, H., Priyadarshani, W., Wijesekera, H. Water mass exchanges between the Bay of Bengal and Arabian Sea from multiyear sampling with autonomous gliders. *Journal of Physical Oceanography*, 2022, 52, 2377–2396, https://doi.org/10.1175/JPO-D-21-0279.1.

Shang, X., Shu, Y., Wang, D., Yu, J., Mao, H., Liu, D., Qiu, C., Tang, H. Submesoscale motions driven by down-front wind around an anticyclonic eddy with a cold core. *Journal of Geophysical Research: Oceans*, 2023, 128, e2022JC019173. https://doi.org/10.1029/2022JC019173.

Sherman, J., Davis, R. E., Owens, W. B. and Valdes, J., 2001. The autonomous underwater glider "Spray", IEEE J. Ocean Eng., 26(4): 437~446.

Shu, Y., Xiu, P., Xue, H., Yao, J., Yu, J. (2016). Glider-observed anticyclonic eddy in northern South China Sea. *Aquatic Ecosystem Health & Managemen*t, 19(3), 233–241. https://doi.org/10.1080/14634988.2016.1208028

Su, D., Lin, P., Mao, H., Wu, J., Liu, H., Cui, Y., Qiu, C. Features of slope intrusion mesoscale eddies in the northern South China Sea. *Journal of Geophysical Research: Oceans,* 2020, 125, e2019JC015349. https://doi.org/ 10.1029/2019JC015349.

Tang, H., Shu, Y., Wang, D., Xie, Q., Zhang, Z., Li, J., Shang, X., Zhang, O., Liu, D. Submesoscale processes observed by high-frequency float in the western South China Sea. *Deep Sea Research Part I: Oceanographic Research Papers*, 2022, 103896. https://doi.org/10.1016/j.dsr.2022.103896

Thomas, L., Taylor, J., Ferrari, R., Terrence M. Symmetric instability in the Gulf Stream. *Deep Sea Research Part II: Topical Studies in Oceanography*, 2013, 91, 96-110. https://doi.org/10.1016/j.dsr2.2013.02.025

Todd, R.E., Ren, A.S. Warming and lateral shift of the Gulf Stream from in situ observations since 2001. *Nature Climate Change,* 2023, **13**, 1348–1352. https://doi.org/10.1038/s41558-023-01835-w

Wang, G., Su, J., Chu, P. Mesoscale eddies in the South China Sea observed with altimetry. *Geophysical Research Letter*, 2003, 30(21), 2121. doi: 10.1029/2003GL018532.

Wang, G., Chen, D., Su, J. Winter eddy genesis in the eastern South China Sea due to orographic wind jets. *Journal of Physical Oceanography*, 2008, 38(3), 726–732. https://doi.org/10.1175/2007jpo3868.1

Wang, Q., Zeng, L., Li, J., Chen, J., He, Y., Yao, J., Wang, D., Zhou, W. Observed Cross-Shelf Flow Induced by Mesoscale Eddies in the Northern South China Sea. *Journal of Physical Oceanography*, 2018, 48, 1609–1628. https://doi.org/10.1175/JPO-D-17-0180.1

Wang, D., Xu, H., Lin, J., Hu, J. Anticyclonic eddies in the northeastern South China Sea during winter of 2003/2004. *Journal of Oceanography*, 2008, 64(6), 925-935

Wang, Z., Chen, Q. Warm core eddies in the northern South China Sea (I): Preliminary observations of warm eddies in the South China Sea. J*ournal of Oceanography of Taiwan Strait*,1987, 18, 92-103.

Wu, J., Zhang, M., Sun, X. Hydrodynamic characteristics of the main parts of a hybrid-driven underwater glider PETREL. InTech, 2011. ISBN: 978-953-307-432-0.

Xu, J., Su, J. Hydrographic analysis of Kuroshio intrusion into the South China Sea II: Observations during UGust-September 1994. *Tropical Oceanography*,1997, 2, 1-23.

Yang, H., Liu, Q. The seasonal features of temperature distributions in the upper layer of the South China Sea. *Oceanologia et Limnologia Sinica*, 1998,29(5), 501-507.

Xiu, P., Chai, F., Shi, L., Xue, H., Chao, Y. A census of eddy activities in the South China Sea during 1993-2007. *Journal of Geophysical Research: Oceans*, 2010,115, C03012. doi: 10.1029/2009JC005657.

Yang, Q., Nikurashin, M., Sasaki, H., Sun, H., Tian, J. Dissipation of mesoscale eddies and its contribution to mixing in the northern South China Sea. *Scientific Reports*, 2019, 9. https://doi.org/10.1038/s41598-018-36610-x

Yi, Z., Wang, D., Qiu, C., Mao, H., Yu, J., Lian, S. Variations in dissolved oxygen induced by a tropical storm within an anticyclone in the Northern South China Sea. *Journal of Ocean University of China*, 2022, 21(5), 1084-1098. https://doi.org/10.1007/s11802-022-4992-4.

Yu, J., Zhang, A, Jing, W. Chen, Q. Tian, Y., Liu, W. Development and Experiments of the Sea-Wing Underwater Glider. *China Ocean Engineering*, 2011, 25(4), 721-736. https://doi.org/10.1007/s13344-011-0058-x.

Zhang, Z., Qiu, B. Evolution of submesoscale ageostrophic motions through the life cycle of oceanic mesoscale eddies. *Geophysical Research Letters,* 2018, 45(21), 11847-11855. https://doi.org/10.1029/2018GL080399

Zhang, Z., Tian, J., Qiu, B., Zhao, W., Chang, P., Wu, D. Observed 3D Structure, Generation, and Dissipation of Oceanic Mesoscale Eddies in the South China Sea. *Scientific Reports,* 2016, 6(1), 24349. https://doi.org/10.1038/srep24349

Zhang, Z., Zhao, W., Qiu, B., Tian, J. Anticyclonic eddy sheddings from Kuroshio loop and the accompanying cyclonic eddy in the Northeastern South China Sea. *Journal of Physical Oceanography*, 2017, 47(6), 1243-1259. https://doi.org/10.1175/JPO-D-16-0185.1